Supplement of Clim. Past, 20, 1303–1325, 2024
https://doi.org/10.5194/cp-20-1303-2024-supplement

Climate of the Past
Open Access
EGU

Supplement of

Polar amplification of orbital-scale climate variability in the early Eocene greenhouse world

Chris D. Fokkema et al.

Correspondence to: Chris D. Fokkema (c.d.fokkema@uu.nl)

Supplementary Figures

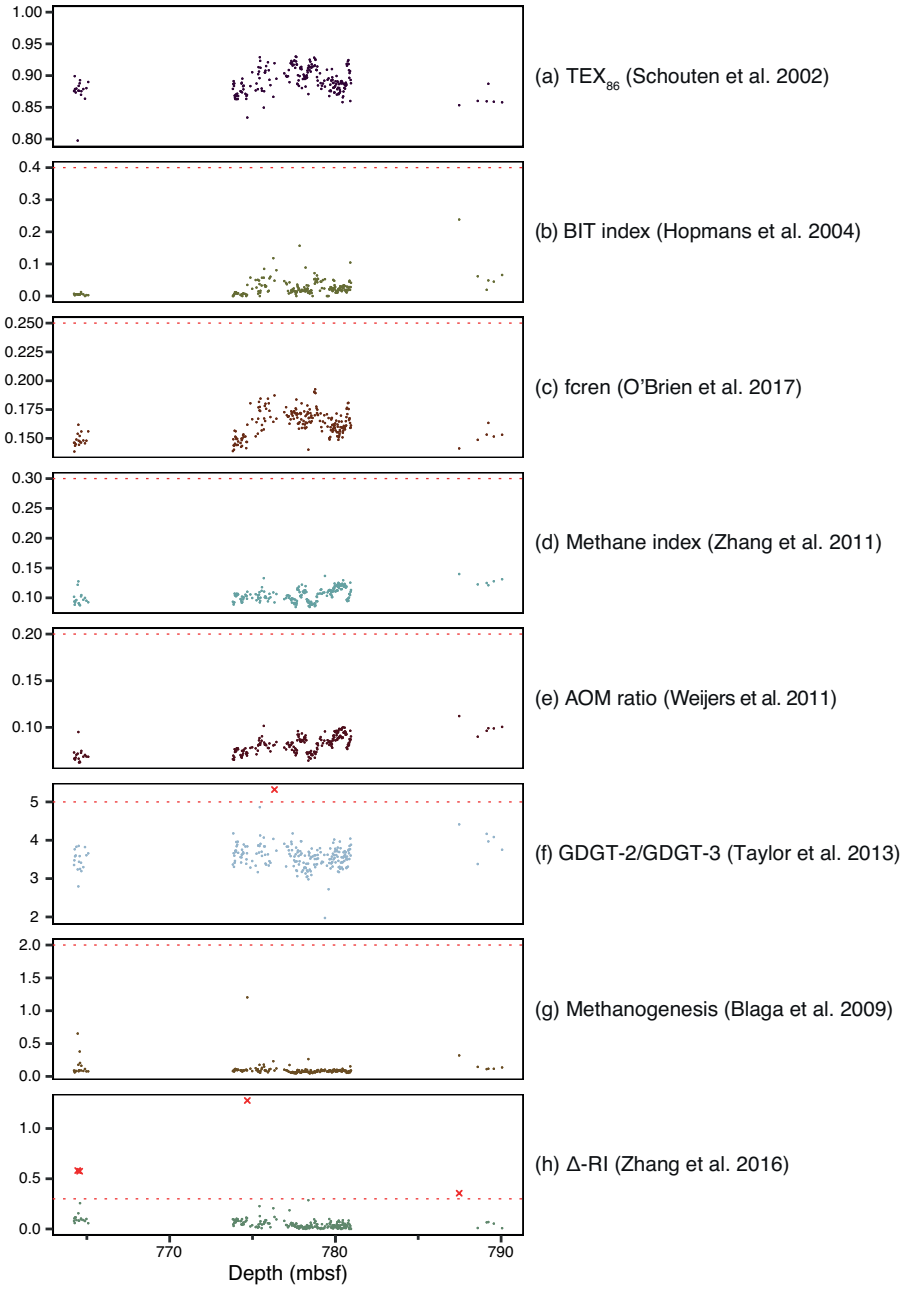

Figure S1. GDGT indices applied to detect possible overprinted TEX_{86} data. Dashed red line indicates cut-off value above which data is discarded as outlier.

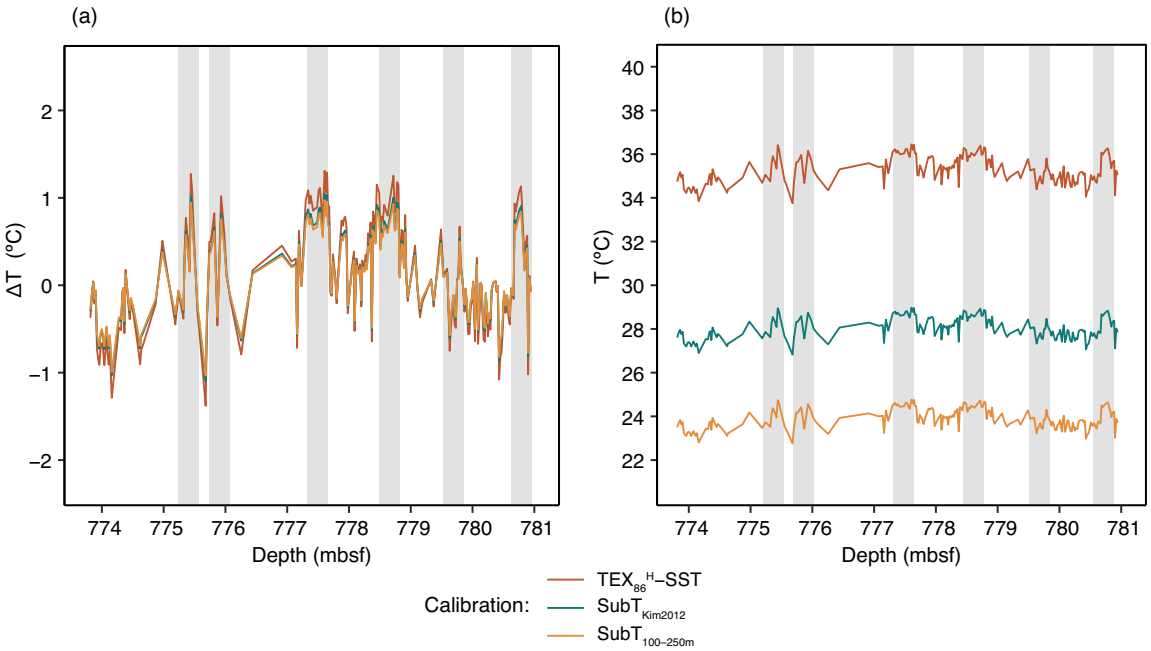

Figure S2. Results of this research using SubT and SST TEX_{86}-temperature calibrations applied to the early Eocene from Site 959. (**a**) Relative temperature changes (ΔT) for multiple calibrations after removing the mean absolute temperature. (**b**) Absolute temperatures for each calibration. Colors correspond to different calibrations.

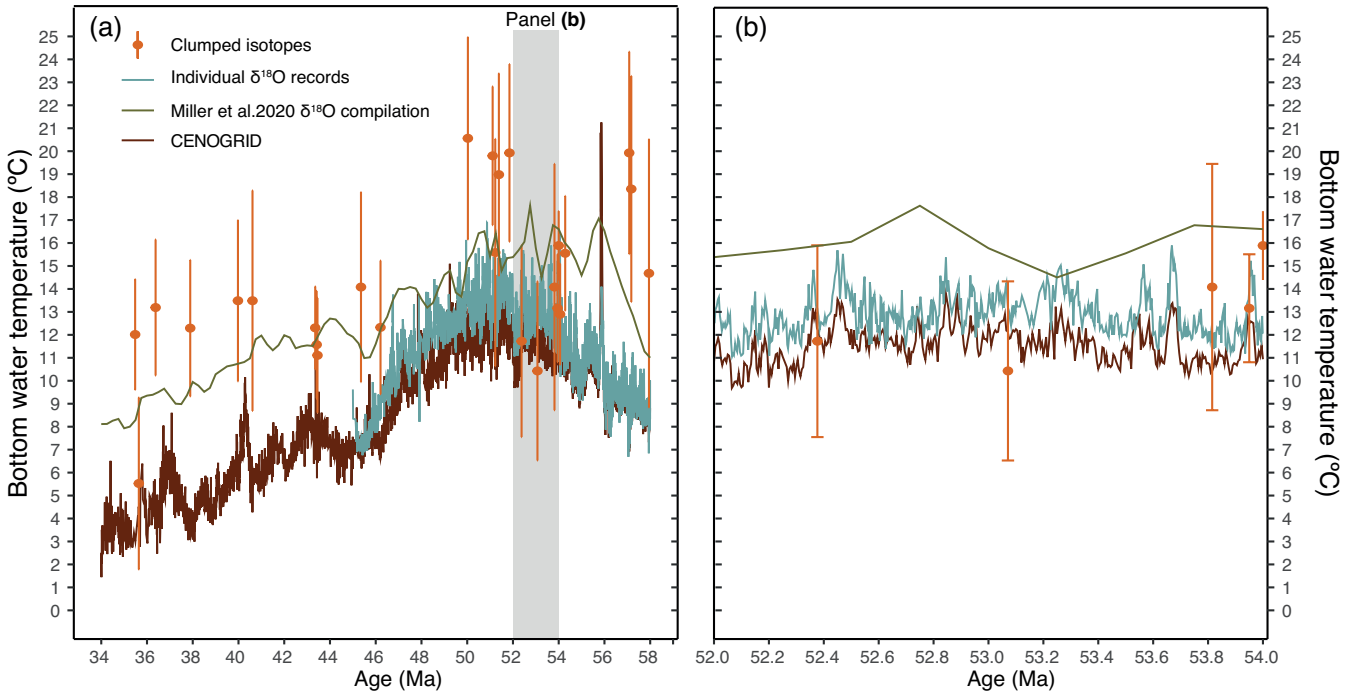

Figure S3. Various bottom water temperature reconstructions spanning the entire Eocene (**a**) and studied interval between 52 and 54 Ma (**b**). The light-blue record is calculated from benthic $\delta^{18}O$ data as reported by Stap et al. (2010), Littler et al. (2014), Lauretano et al. (2015, 2018), Westerhold et al. (2018) and Thomas et al. (2018). Orange datapoints with vertical lines represent clumped isotope-based temperatures with mean (points) and 95% confidence intervals (bars) (Meckler et al., 2022). Brown line indicates CENOGRID benthic compilation (Westerhold et al., 2020) and the green line shows the data from the Miller et al. (2020**)** compilation.

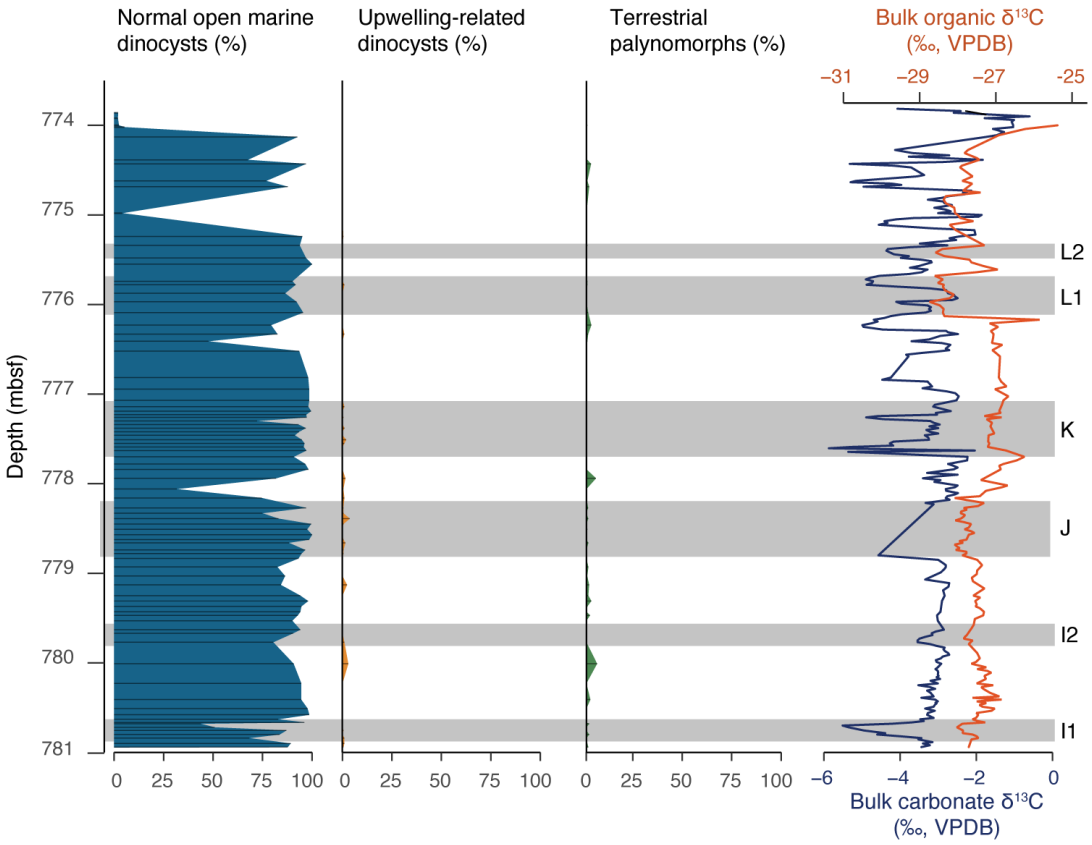

Figure S4. Palynological assemblages of Site 959 Core 39R. Relative abundance of dinocyst groups of normal marine (including *Spiniferites* complex, fibrous Cribroperidinioids, *Operculodinium*, *Florentinia*) and upwelling affinity (i.e., protoperidinioids) and terrestrial palynomorphs (i.e., pollen and spores). On the right bulk organic (orange) and carbonate (dark blue) carbon isotope results, with globally recognized carbon isotope excursions marked by grey bars.

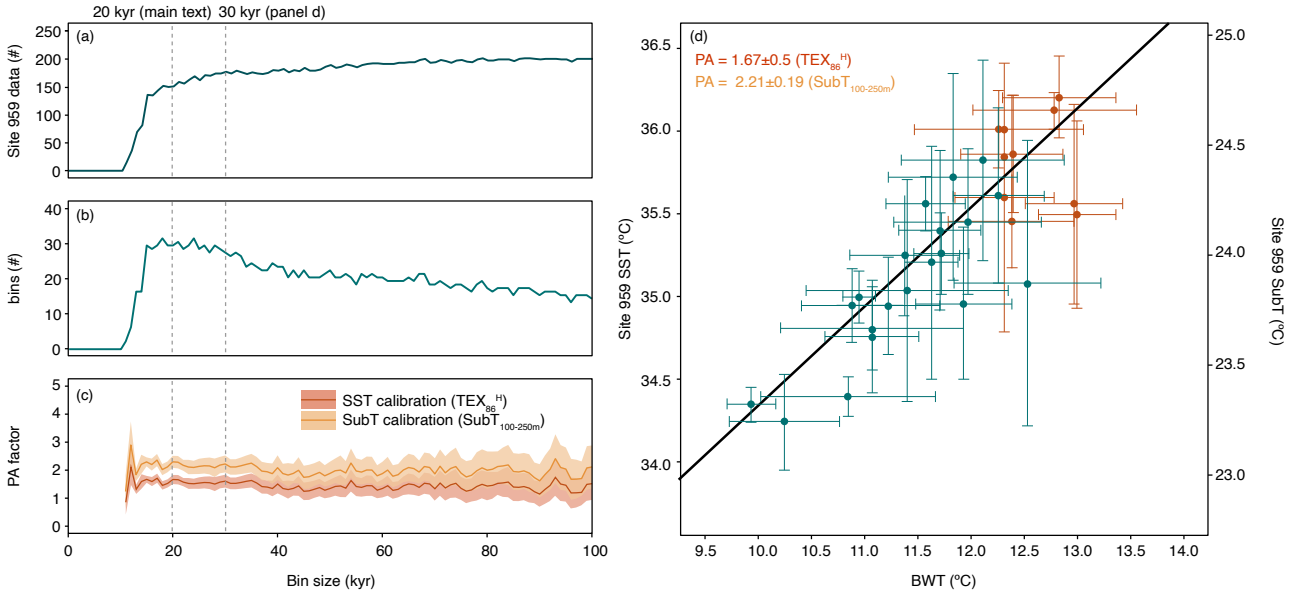

Figure S5. Bin size sensitivity analysis for PA calculation. (**a**) Number of Site 959 TEX_{86} data incorporated in the analysis, (**b**) number of bins, based on a minimum of 3 datapoints per bin and (**c**) PA factor and associated error, after calibrating Site 959 TEX_{86} data to SST (red) or SubT (orange). (**b**) Visualization of PA calculation using a bin size of 30-kyr, following the same procedure as for Fig. 5c in the main text. The dashed lines in panels (**a**–**c**) indicates the bin size of 20-kyr that is applied in the calculation of PA as presented in the main text, and that of 30-kyr as utilized to calculate PA in panel (**d**).

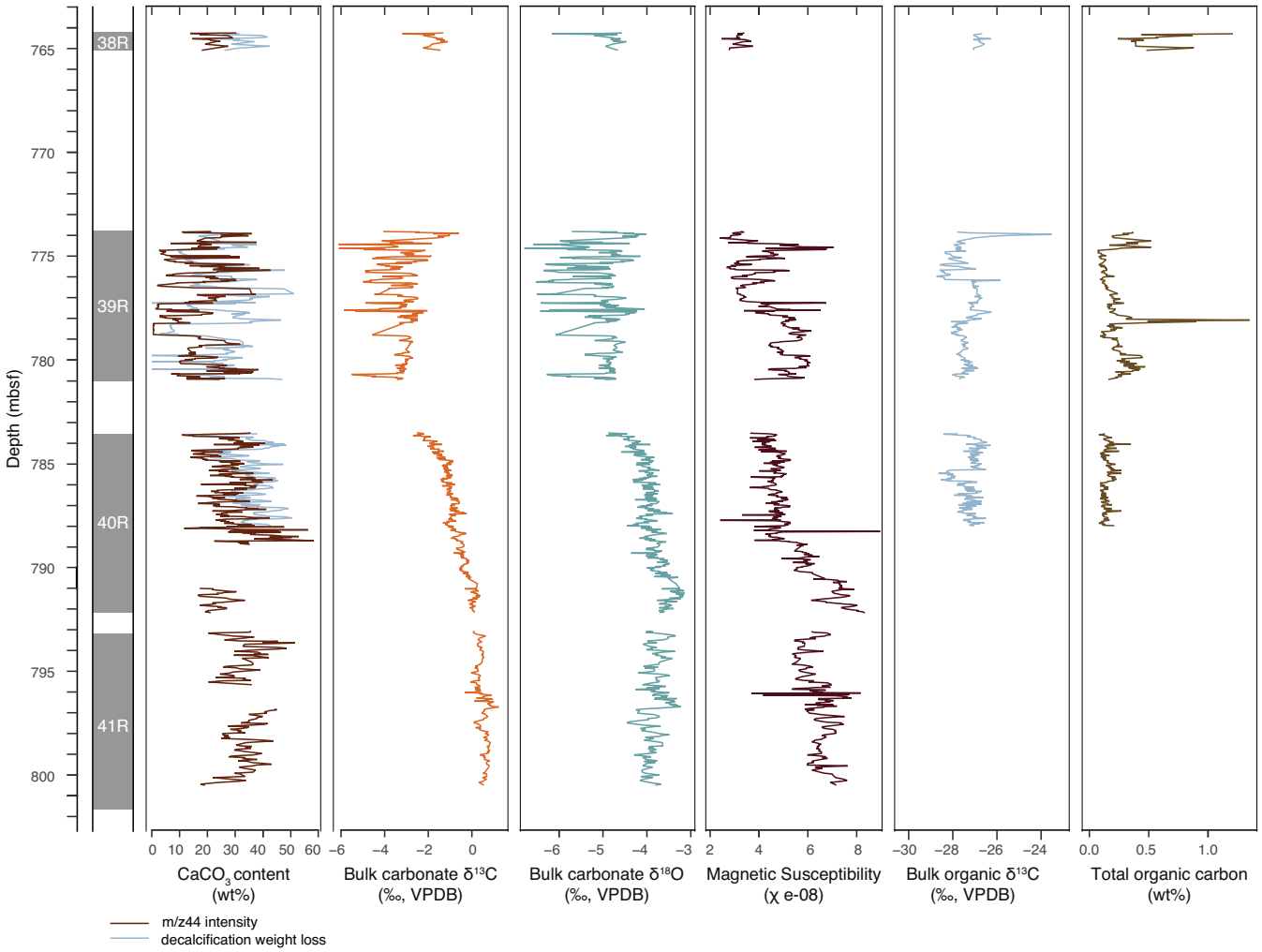

Figure S6. Bulk sediment analysis results from Site 959D Cores 41R – 38R. From left to right: $CaCO_3$ weight percent (wt%), bulk carbonate $\delta^{13}C$, bulk carbonate $\delta^{18}O$, magnetic susceptibility, bulk organic carbon $\delta^{13}C$, TOC wt% and isoprenoid GDGT concentrations.

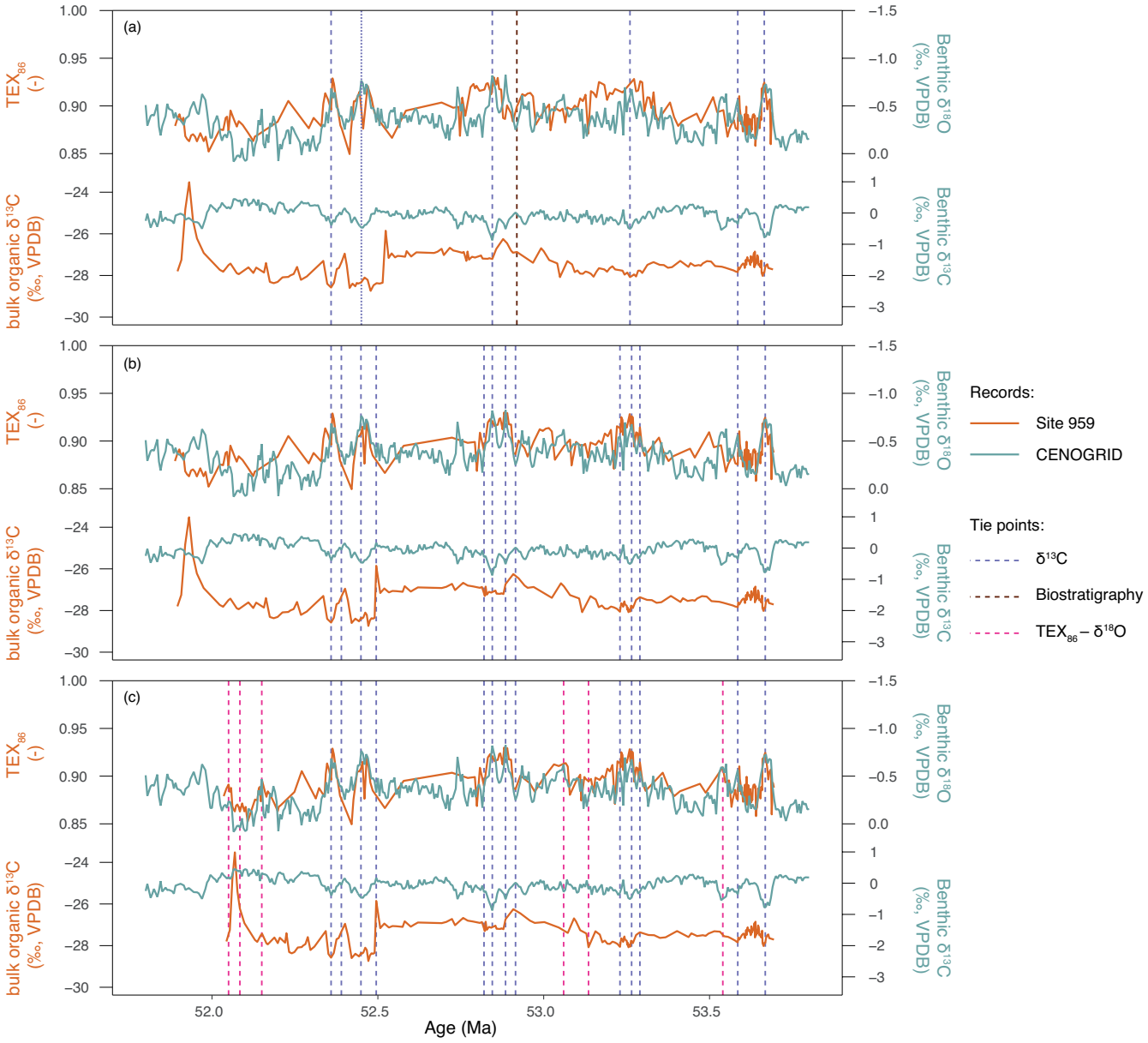

55 **Figure S7**. Finetuned correlation of Site 959 Core 39R TEX_{86} and $\delta^{13}C$ record to CENOGRID benthic $\delta^{18}O$ and $\delta^{13}C$ records (Westerhold et al., 2020) for direct comparison of climate variability. (**a**) Initial correlation between Site 959 (orange) and CENOGRID (green) records based on biostratigraphy and CIEs. (**b**) Same as (**a**), but finetuned using detailed $\delta^{13}C_{org}$ ties. (**c**) Same as (**b**), but with additional correlations between Site 959 TEX_{86} and CENOGRID benthic $\delta^{18}O$, to optimize for direct comparison between the two climate records. Vertical dashed lines represent used tie points.

60

Supplementary References

Blaga, C. I., Reichart, G.-J., Heiri, O., and Sinninghe Damsté, J. S.: Tetraether membrane lipid distributions in water-column particulate matter and sediments: a study of 47 European lakes along a north–south transect, J Paleolimnol, 41, 523–540, https://doi.org/10.1007/s10933-008-9242-2, 2009.

Ho, S. L. and Laepple, T.: Flat meridional temperature gradient in the early Eocene in the subsurface rather than surface ocean, Nature Geosci, 9, 606–610, https://doi.org/10.1038/ngeo2763, 2016.

Hopmans, E. C., Weijers, J. W. H., Schefuß, E., Herfort, L., Sinninghe Damsté, J. S., and Schouten, S.: A novel proxy for terrestrial organic matter in sediments based on branched and isoprenoid tetraether lipids, Earth Planet. Sc. Lett., 224, 107–116, https://doi.org/10.1016/j.epsl.2004.05.012, 2004.

Kim, J.-H., van der Meer, J., Schouten, S., Helmke, P., Willmott, V., Sangiorgi, F., Koç, N., Hopmans, E. C., and Damsté, J. S. S.: New indices and calibrations derived from the distribution of crenarchaeal isoprenoid tetraether lipids: Implications for past sea surface temperature reconstructions, Geochim. et Cosmochim., 74, 4639–4654, https://doi.org/10.1016/j.gca.2010.05.027, 2010.

Kim, J.-H., Romero, O. E., Lohmann, G., Donner, B., Laepple, T., Haam, E., and Sinninghe Damsté, J. S.: Pronounced subsurface cooling of North Atlantic waters off Northwest Africa during Dansgaard–Oeschger interstadials, Earth and Planetary Science Letters, 339–340, 95–102, https://doi.org/10.1016/j.epsl.2012.05.018, 2012.

Lauretano, V., Littler, K., Polling, M., Zachos, J. C., and Lourens, L. J.: Frequency, magnitude and character of hyperthermal events at the onset of the Early Eocene Climatic Optimum, Clim. Past, 11, 1313–1324, https://doi.org/10.5194/cp-11-1313-2015, 2015.

Lauretano, V., Zachos, J. C., and Lourens, L. J.: Orbitally Paced Carbon and Deep-Sea Temperature Changes at the Peak of the Early Eocene Climatic Optimum, Paleoceanogr. and Paleoclimatol., 33, 1050–1065, https://doi.org/10.1029/2018PA003422, 2018.

Littler, K., Röhl, U., Westerhold, T., and Zachos, J. C.: A high-resolution benthic stable-isotope record for the South Atlantic: Implications for orbital-scale changes in Late Paleocene–Early Eocene climate and carbon cycling, Earth Planet. Sc. Lett., 401, 18–30, https://doi.org/10.1016/j.epsl.2014.05.054, 2014.

Meckler, A. N., Sexton, P. F., Piasecki, A. M., Leutert, T. J., Marquardt, J., Ziegler, M., Agterhuis, T., Lourens, L. J., Rae, J. W. B., Barnet, J., Tripati, A., and Bernasconi, S. M.: Cenozoic evolution of deep ocean temperature from clumped isotope thermometry, Science, 377, 86–90, https://doi.org/10.1126/science.abk0604, 2022.

O'Brien, C. L., Robinson, S. A., Pancost, R. D., Sinninghe Damsté, J. S., Schouten, S., Lunt, D. J., Alsenz, H., Bornemann, A., Bottini, C., Brassell, S. C., Farnsworth, A., Forster, A., Huber, B. T., Inglis, G. N., Jenkyns, H. C., Linnert, C., Littler, K., Markwick, P., McAnena, A., Mutterlose, J., Naafs, B. D. A., Püttmann, W., Sluijs, A., van Helmond, N. A. G. M., Vellekoop, J., Wagner, T., and Wrobel, N. E.: Cretaceous sea-surface temperature evolution: Constraints from TEX86 and planktonic foraminiferal oxygen isotopes, Earth-Sci. Rev., 172, 224–247, https://doi.org/10.1016/j.earscirev.2017.07.012, 2017.

Schouten, S., Hopmans, E. C., Schefuß, E., and Sinninghe Damsté, J. S.: Distributional variations in marine crenarchaeotal membrane lipids: a new tool for reconstructing ancient sea water temperatures?, Earth Planet. Sc. Lett., 204, 265–274, https://doi.org/10.1016/S0012-821X(02)00979-2, 2002.

Stap, L., Lourens, L. J., Thomas, E., Sluijs, A., Bohaty, S., and Zachos, J. C.: High-resolution deep-sea carbon and oxygen isotope records of Eocene Thermal Maximum 2 and H2, Geology, 38, 607–610, https://doi.org/10.1130/G30777.1, 2010.

Taylor, K. W. R., Huber, M., Hollis, C. J., Hernandez-Sanchez, M. T., and Pancost, R. D.: Re-evaluating modern and Palaeogene GDGT distributions: Implications for SST reconstructions, Global Planet. Change, 108, 158–174, https://doi.org/10.1016/j.gloplacha.2013.06.011, 2013.

Thomas, E., Boscolo-Galazzo, F., Balestra, B., Monechi, S., Donner, B., and Röhl, U.: Early Eocene Thermal Maximum 3: Biotic Response at Walvis Ridge (SE Atlantic Ocean), Paleoceanogr. Paleoclimatol., 33, 862–883, https://doi.org/10.1029/2018PA003375, 2018.

Weijers, J. W. H., Lim, K. L. H., Aquilina, A., Sinninghe Damsté, J. S., and Pancost, R. D.: Biogeochemical controls on glycerol dialkyl glycerol tetraether lipid distributions in sediments characterized by diffusive methane flux, Geochem. Geophys. Geosyst., 12, Q10010, https://doi.org/10.1029/2011GC003724, 2011.

Westerhold, T., Röhl, U., Donner, B., and Zachos, J. C.: Global Extent of Early Eocene Hyperthermal Events: A New Pacific Benthic Foraminiferal Isotope Record From Shatsky Rise (ODP Site 1209), Paleoceanogr. Paleoclimatol., 33, 626–642, https://doi.org/10.1029/2017PA003306, 2018.

Westerhold, T., Marwan, N., Drury, A. J., Liebrand, D., Agnini, C., Anagnostou, E., Barnet, J. S. K., Bohaty, S. M., De Vleeschouwer, D., Florindo, F., Frederichs, T., Hodell, D. A., Holbourn, A. E., Kroon, D., Lauretano, V., Littler, K., Lourens, L. J., Lyle, M., Pälike, H., Röhl, U., Tian, J., Wilkens, R. H., Wilson, P. A., and Zachos, J. C.: An astronomically dated record of Earth's climate and its predictability over the last 66 million years, Science, 369, 1383–1387, https://doi.org/10.1126/science.aba6853, 2020.

Zhang, Y. G., Zhang, C. L., Liu, X.-L., Li, L., Hinrichs, K.-U., and Noakes, J. E.: Methane Index: A tetraether archaeal lipid biomarker indicator for detecting the instability of marine gas hydrates, Earth Planet. Sc. Lett., 307, 525–534, https://doi.org/10.1016/j.epsl.2011.05.031, 2011.

Zhang, Y. G., Pagani, M., and Wang, Z.: Ring Index: A new strategy to evaluate the integrity of TEX 86 paleothermometry, Paleoceanography, 31, 220–232, https://doi.org/10.1002/2015PA002848, 2016.